

Supplementary material

Sorption-tree with scalable hygroscopic adsorbent-leaves for water harvesting

*Fangfang Deng, Chengjie Xiang, Chenxi Wang, Ruzhu Wang**

Institute of Refrigeration and Cryogenics, Shanghai Jiao Tong University, Shanghai
200040, China

E-mail: rzwang@sjtu.edu.cn

This word file includes:

Fig S1 to Fig S35

Table S1 to S6

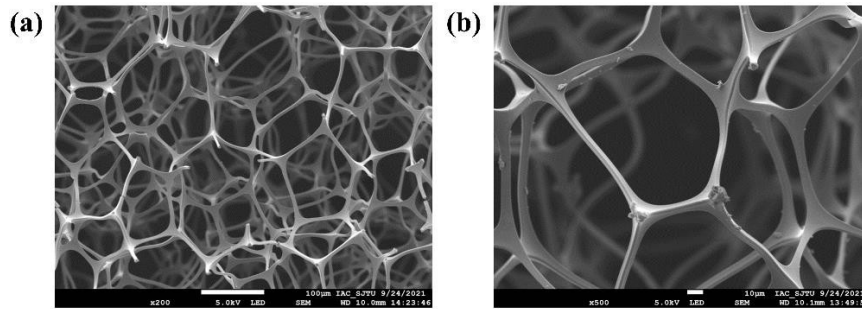


Fig S1. The SEM images of porous structure in raw melamine foam (MF) in different magnification (a) 200×; (b) 500×.

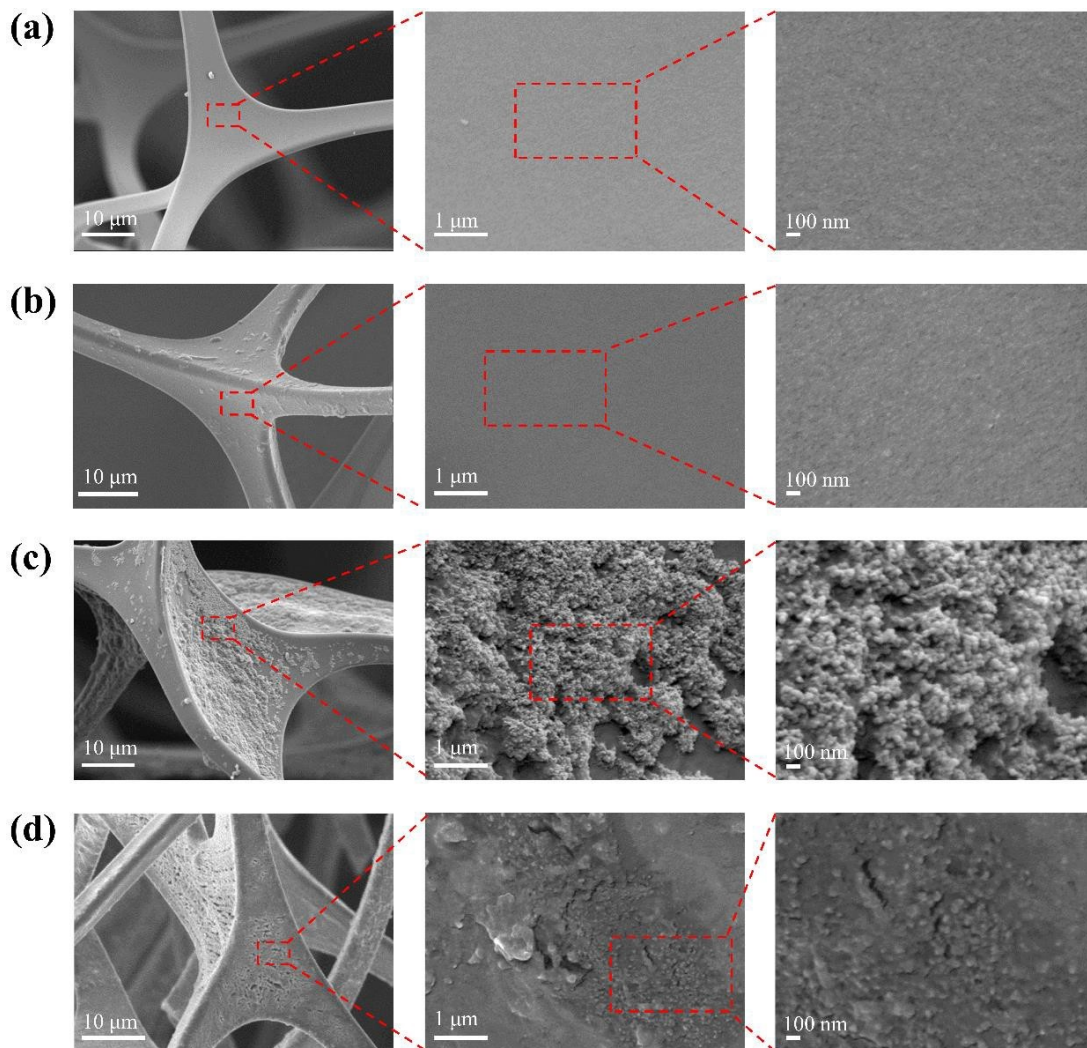


Fig S2. The SEM images of stem's surface of (a)MF; (b)melamine foam grafted sodium alginate (MFSA); (c)melamine foam grafted sodium alginate with carbon ink (IMFSA); (d)melamine foam grafted calcium alginate with carbon ink (IMFCA) in different magnification. The coarse surfaces of IMFSA and IMFCA exist plenty of 20-50 nm nano particles which are predicted to be the carbon nanospheres. At the same time, the surfaces of MF and MFSA is a little flatter.

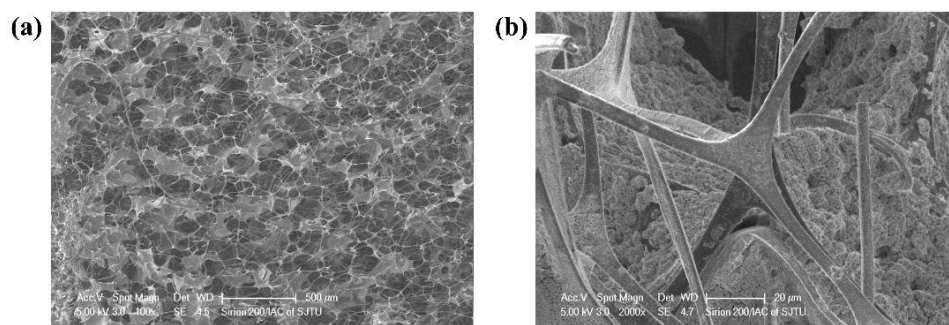


Fig S3. The SEM images of IMFCA in different magnification (a) 100×; (b)2000×. They separately show the morphology structure of IMFCA, in which the salt particles can be observed.

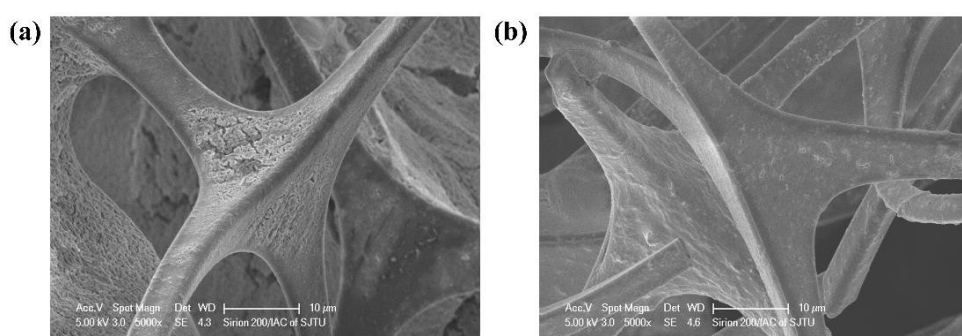


Fig S4. The SEM images of (a)IMFCA and (b)MFCA in the same magnification. The surface of the stem in IMFCA is rougher than that in MFCA, attributed to the load of carbon nanosphere in IMFCA. In addition, the salt particles are adhered to the surface of melamine foam's stems.

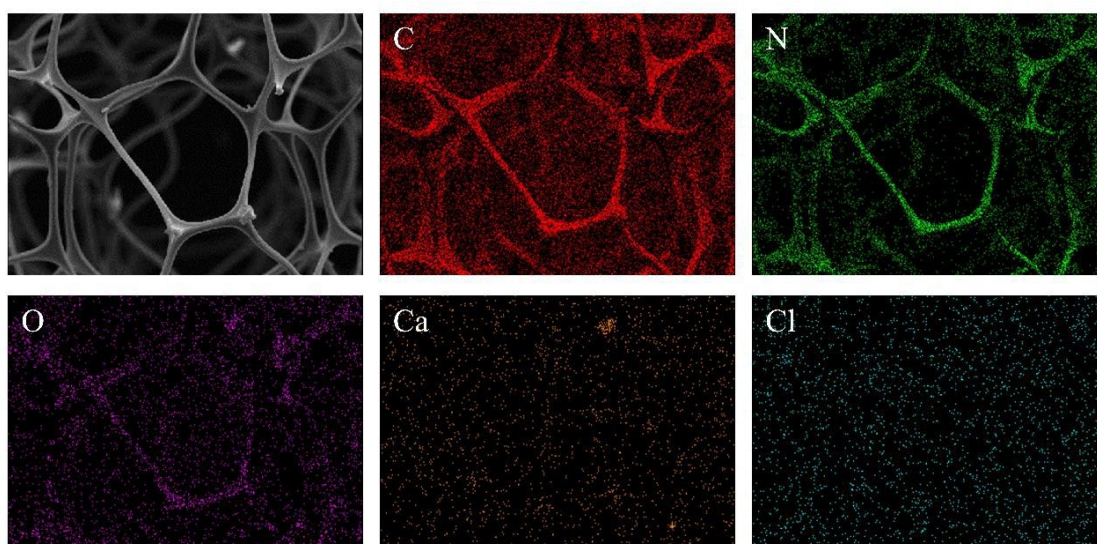


Fig S5. The EDS images of raw MF. It is mainly composed of C and N elements nearly without the Ca and Cl elements.

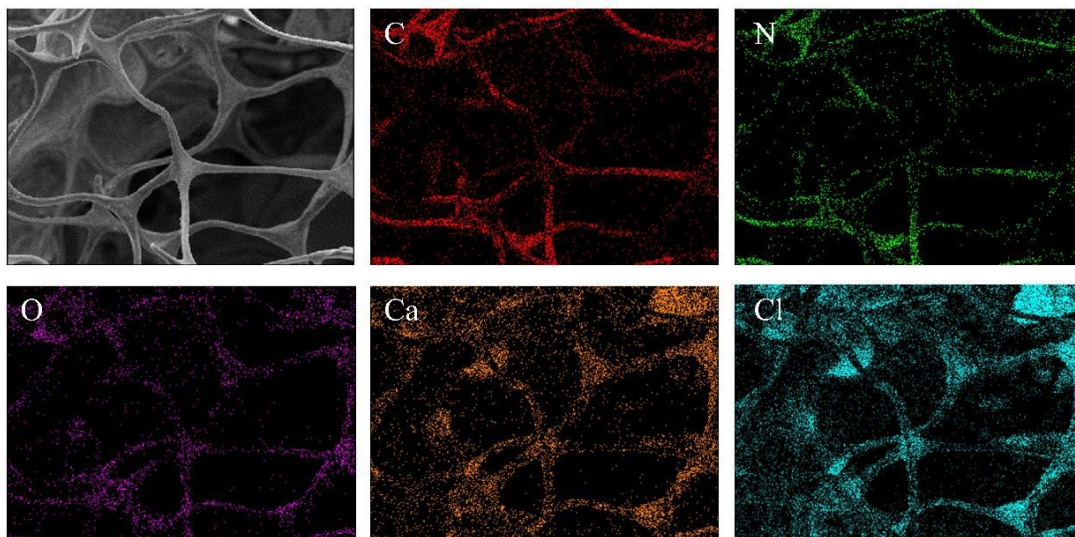


Fig S6. The EDS images of IMFCA. IMFCA is mainly composed of C, N, O, Ca and Cl elements, among which the Ca and Cl elements are derived from the CaCl_2 salt particles. A part of dispersed salts is impregnated in the calcium alginate gel wrapping on the IMFCA's stems; the other part is impregnated in the pores of melamine foam with the help of capillary action.

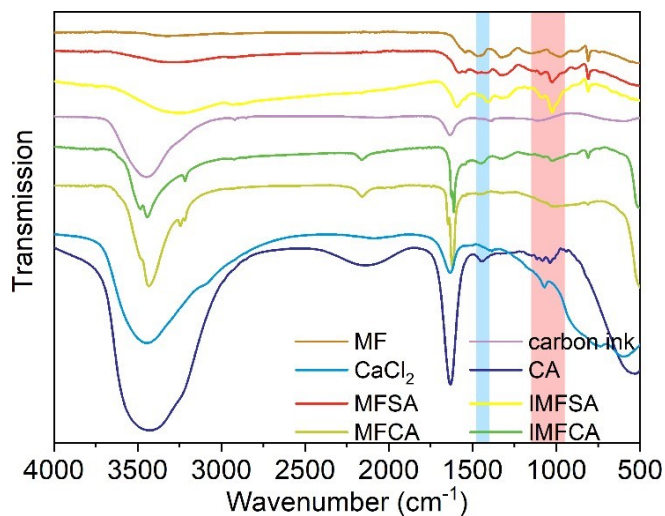


Fig S7. The FTIR results of IMFCA, IMFSA, MFCA, MFSA, CA, MF, CaCl_2 and carbon ink. These diagrams show the transmission related to wavenumber. The spectrum of IMFCA is similar to that of MFCA, and the spectrum of IMFSA is similar to that of MFSA. Except for raw MF, CaCl_2 , and carbon ink, the typical $-\text{COOH}$ group in CA (vibrations at $1400\text{-}1450\text{ cm}^{-1}$) is presented in the corresponding wavenumbers of MFCA and IMFCA, which suggests the containment of CA in IMFCA and MFCA.

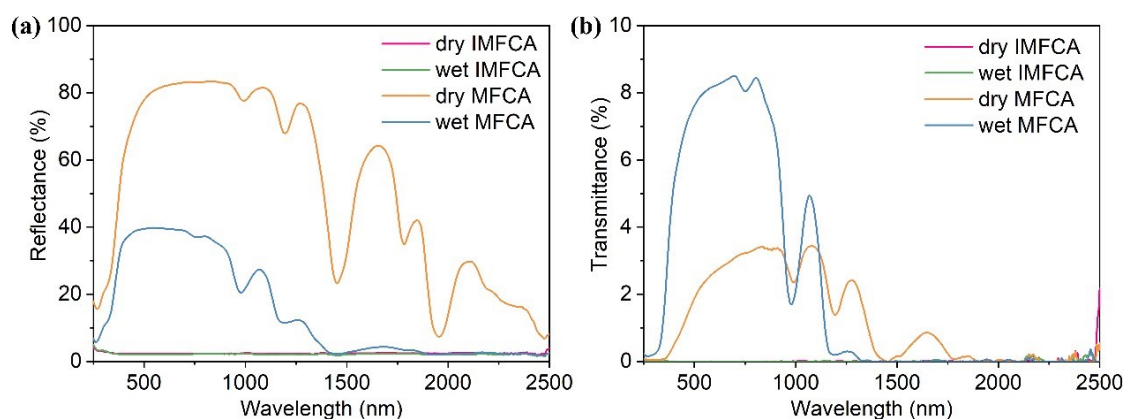


Fig S8. The UV-vis-nIR results of IMFCA and MFCA with wet and dry states. (a) the sunlight reflectance of four samples; (b) the sunlight transmittance of four samples.

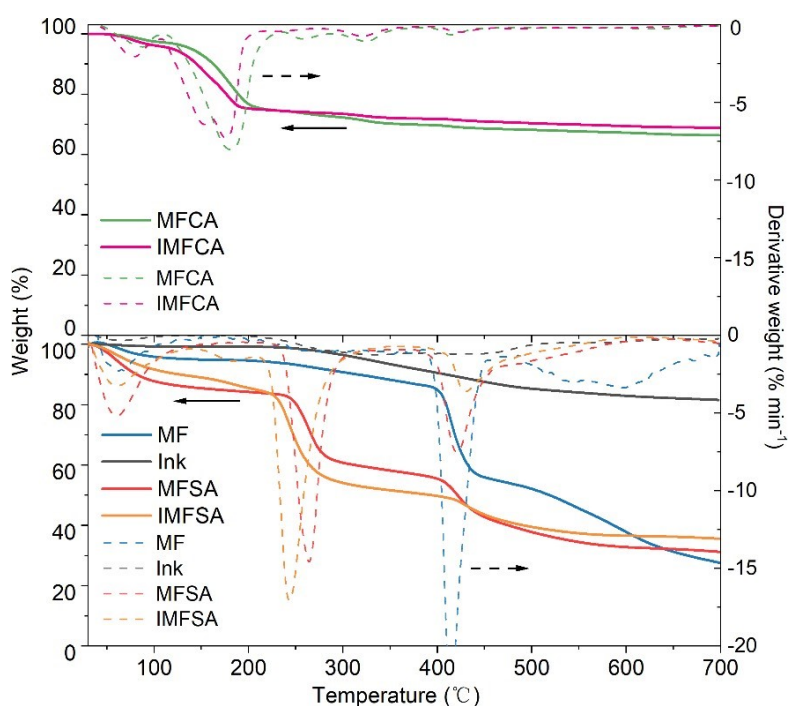


Fig S9. The TGA results of IMFCA, MFCA, IMFSA, MFSA, MF and Ink. The temperature rises up from 30 °C to 700 °C with the heating rate of 20 °C min⁻¹. The TGA diagrams of MFCA and IMFCA are similar, as well as the diagrams of MFSA and MFCA, which means that addition of carbon ink has little influence on sample's thermal stability. Compared with MFCA, the diagram of IMFCA shifts left a little, indicating its higher conductivity and faster heat transfer property. Below 200 °C, the hygroscopic IMFCA just loses free water, which verifies the excellent stability of IMFCA in daily operation (the temperature is usually below 120 °C). Between 230 to 700 °C, the largest pyrolysis peak of IMFSA represents the organic pyrolysis process of CA and MF, while IMFCA hardly loses weight (the mass change is below ~6%). Up to 700 °C, ~ 69% of the weight for IMFCA is remained, which is mainly composed of CaCl₂ and carbon ink.

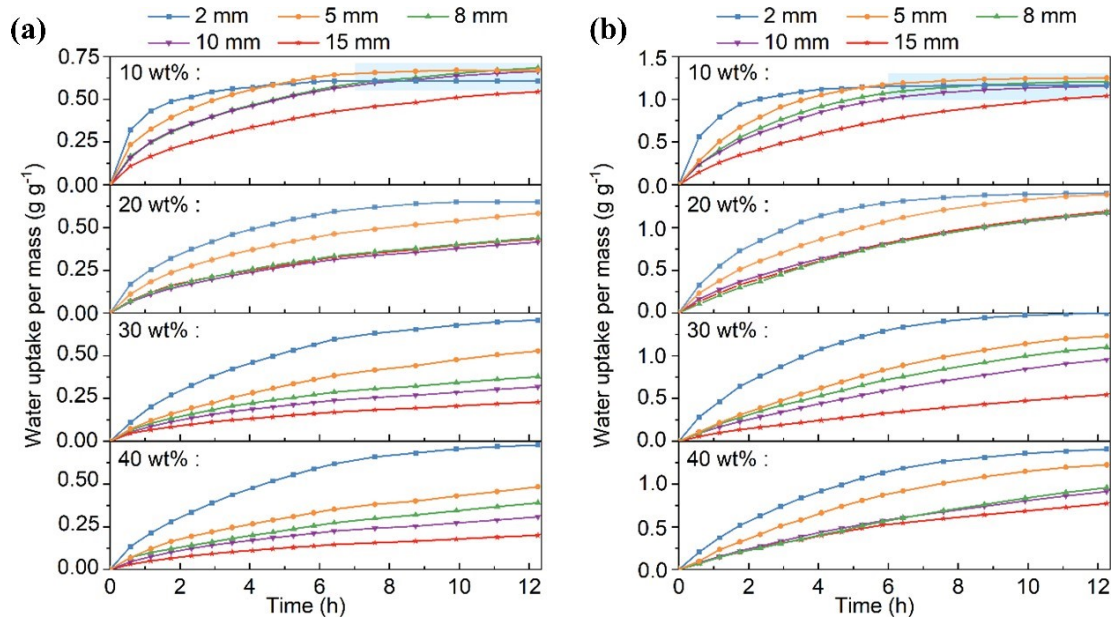


Fig S10. The adsorption performance for several IMFCAs with different thickness and different immersed CaCl_2 concentration.

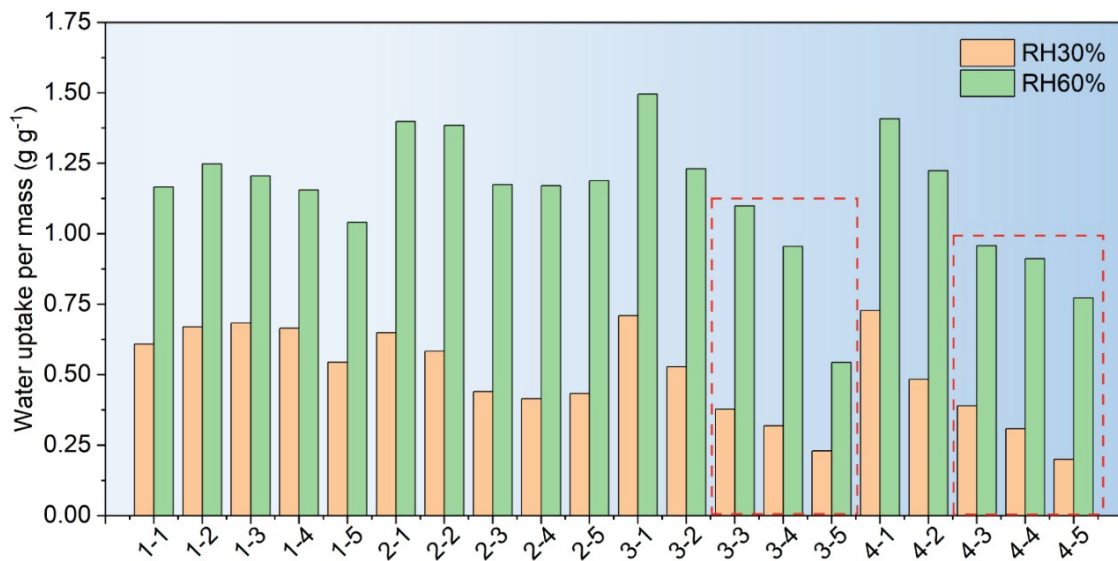


Fig S11. The adsorption performance for 20 kind of samples at 25 °C and RH 30%/RH60%. The vertical axis represents the water uptake per mass of IMFCA. The abscissa axis represents different samples. “m-n” at the abscissa axis means the m^{th} kind of immersed concentration of CaCl_2 solution and the n^{th} kind of thickness. The m changes from 1, 2, 3, 4, which separately means 10 wt.%, 20 wt.%, 30 wt.% and 40 wt.% of the immersed concentration of salty solution. In a similar way, the n changes from 1, 2, 3, 4, 5, which separately means 2 mm, 5 mm, 8 mm, 10 mm and 15 mm of the sample’s thickness.

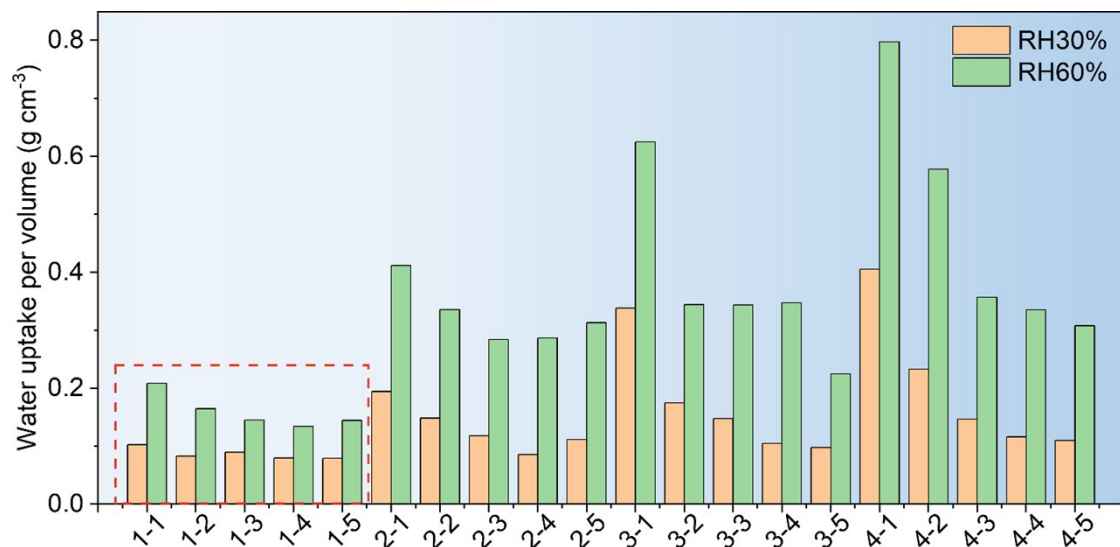


Fig S12. The adsorption performance for 20 kind of samples at 25 °C and RH 30%/RH60%. The vertical axis represents the water uptake per volume of IMFCA. The abscissa axis represents different samples. The meaning of “m-n” at the abscissa axis is the same as Figure S10.

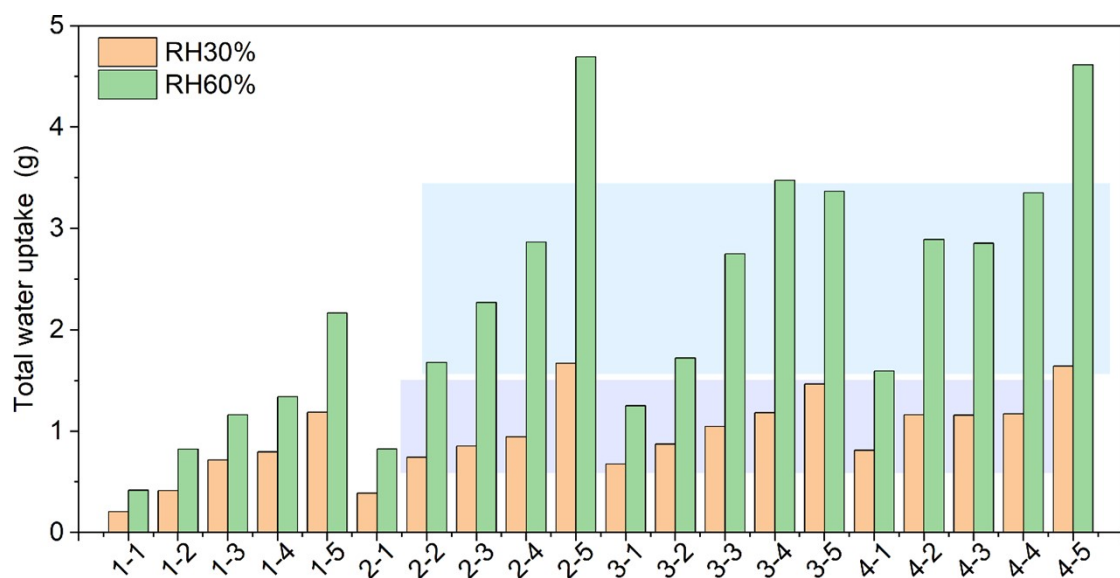


Fig S13. The adsorption performance for 20 kind of samples at 25 °C and RH 30%/RH60%. The vertical axis represents total water uptake of IMFCA. The abscissa axis represents different samples. The meaning of “m-n” at the abscissa axis is the same as Figure S10.

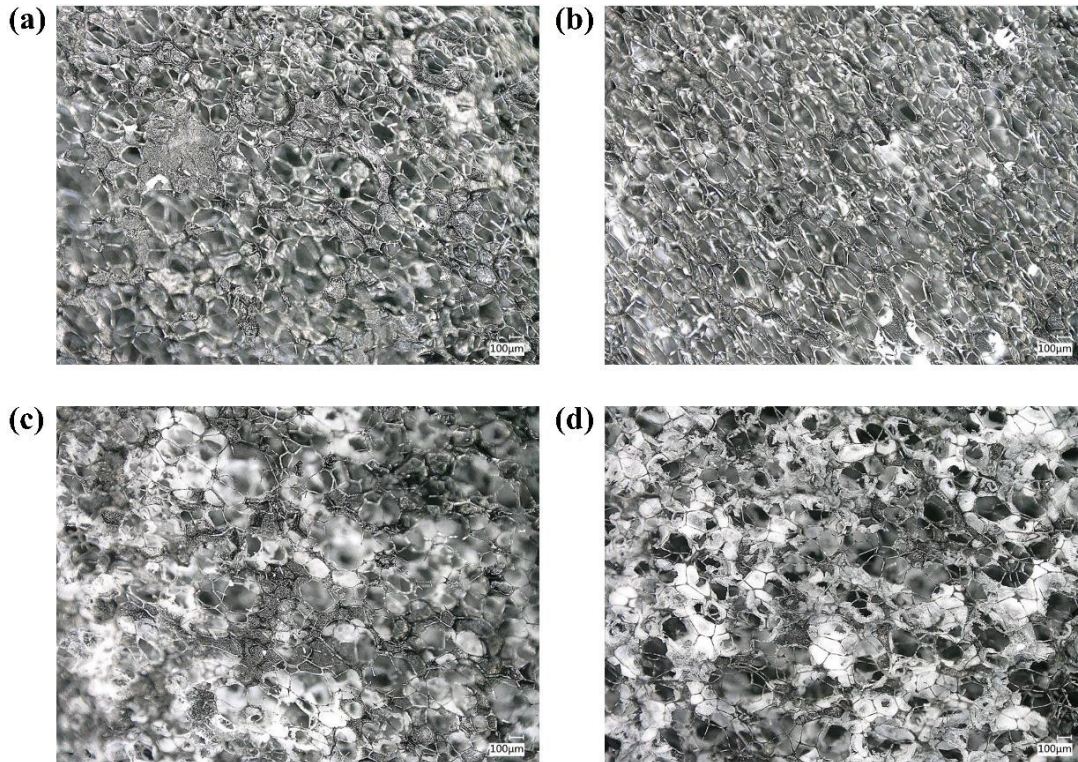


Fig S14. The optical micrographs of IMFCA with different immersed concentration of CaCl_2 solution (10 wt.%, 20 wt.%, 30 wt.%, 40 wt.%). They show the dispersed degree of CaCl_2 particles in the IMFCA's porous structure.

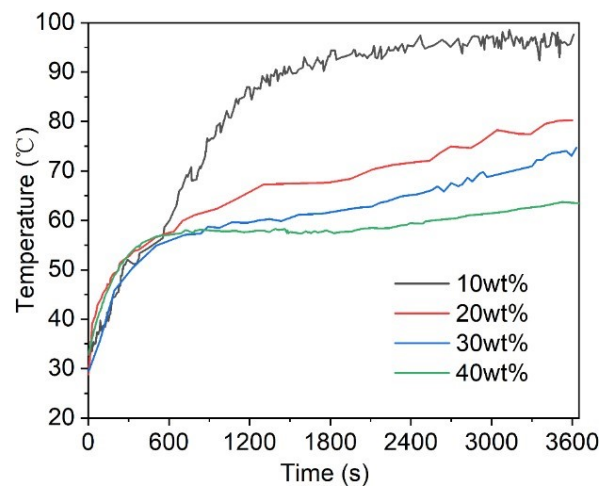


Fig S15. The temperature of the IMFCAs with different immersed concentration of salty solution in 1 h of desorption process. During first 10 minutes, the temperature of IMFCA rapidly increases. After that, the upward trend is tent to be slow until the static temperature is reached.

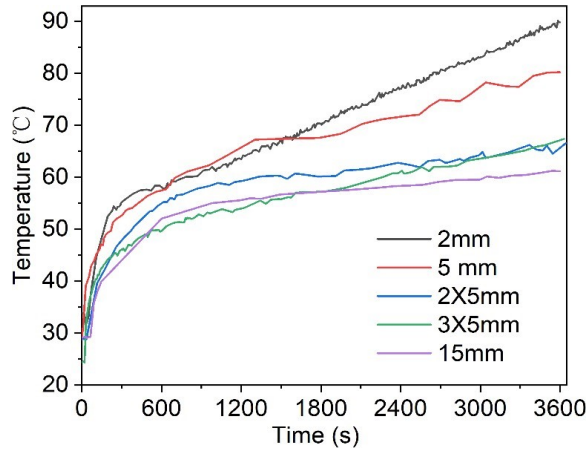


Fig S16. The temperature of the IMFCAs with different thickness in 1 h of desorption process.

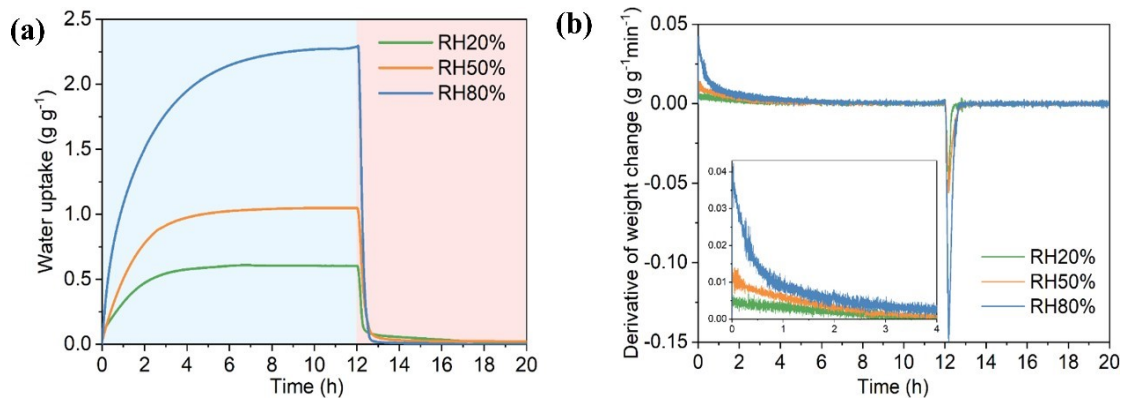


Fig S17. The adsorption-desorption performance of IMFCA in STA at 30 °C and RH 20% & RH 50% & RH 80%. (a) the water uptake for IMFCA; (b) the derivative of mass change for IMFCA.

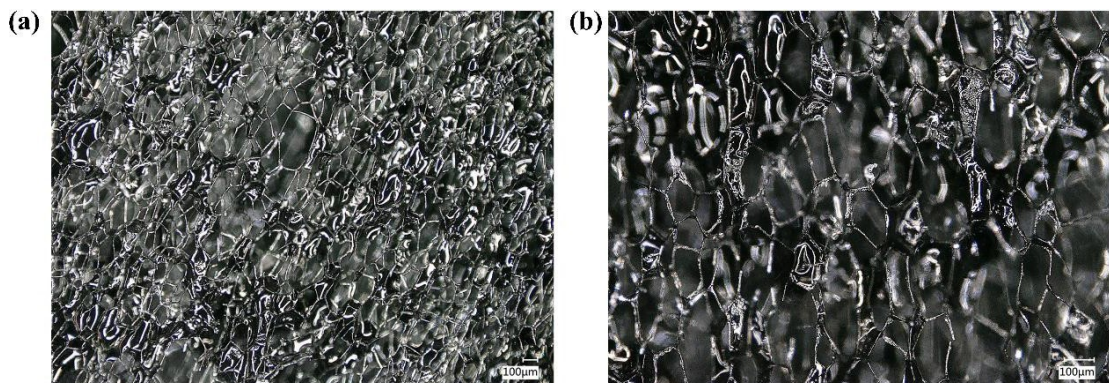


Fig S18. The optical micrographs of hydrated IMFCA after adsorption process. They show the hydrated state of IMFCA, in which the adsorbed water is reserved in the pores of the melamine foam skeleton with the help of capillary action.

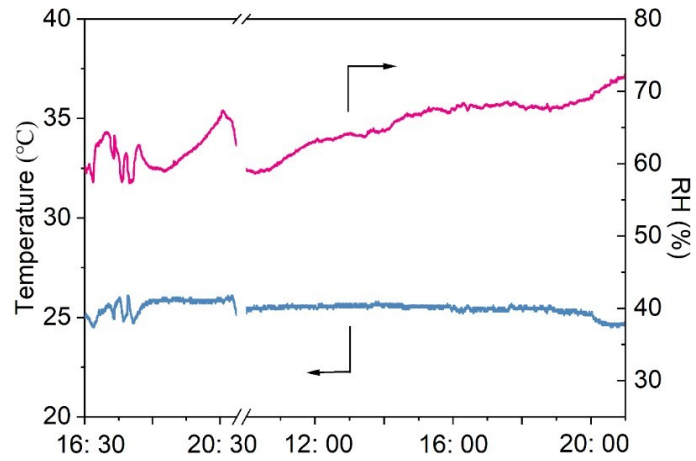


Fig S19. The temperature and the relative humidity in the laboratory when the desorption experiment is carrying on.

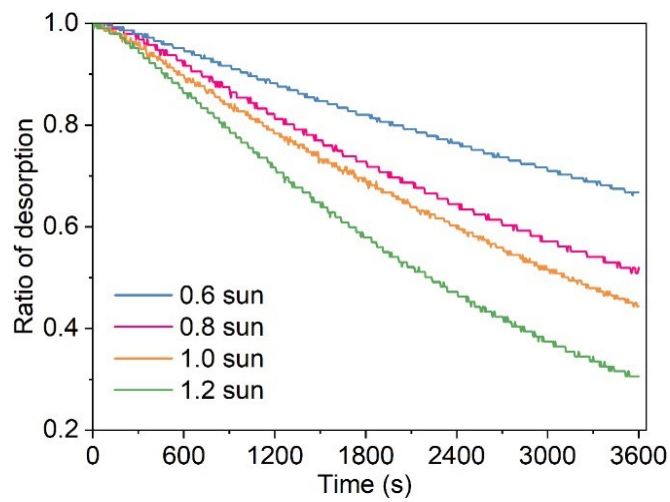


Fig S20. The desorption performance for IMFCA in different solar irradiation intensity (0.6 sun, 0.8 sun, 1 sun, 1.2 sun).

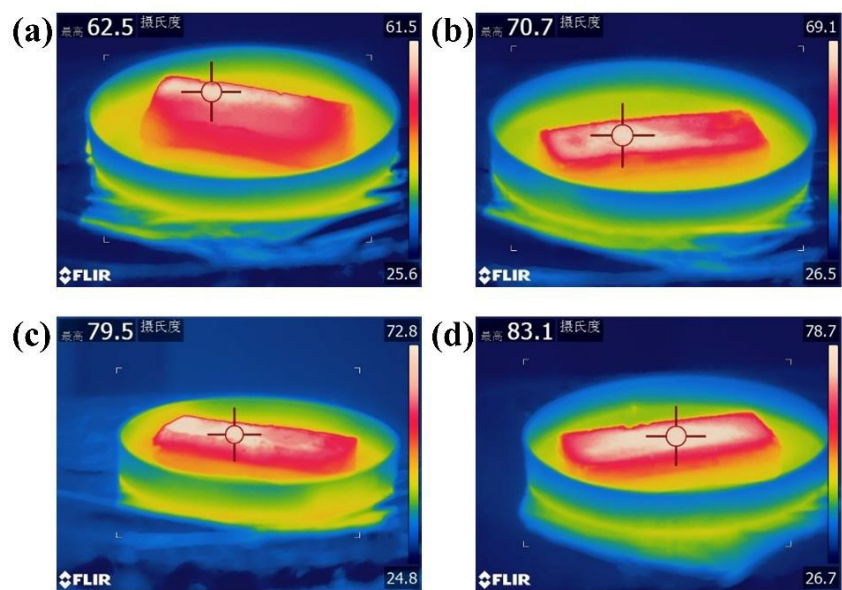


Fig S21. The IR photographs of IMFCAs with the solar irradiation intensity of (a) 0.6 sun, (b) 0.8 sun, (c) 1 sun, and (d) 1.2 sun. They show the temperature distribution of sample's surface when exposed to the sunlight.

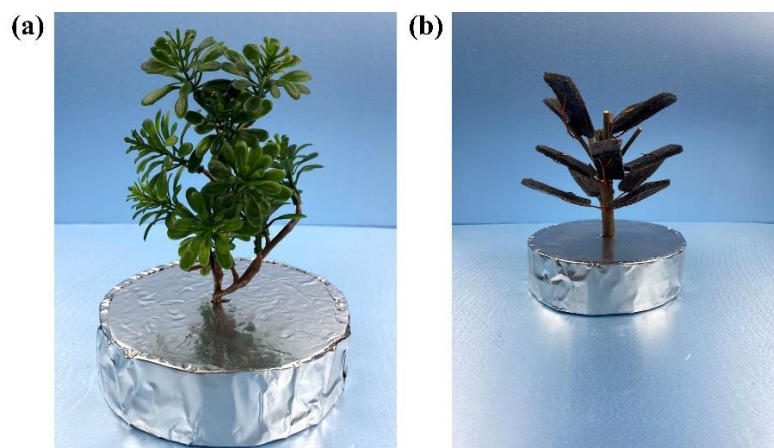


Fig S22. The photographs of artificial ornamental tree and the "sorption tree".

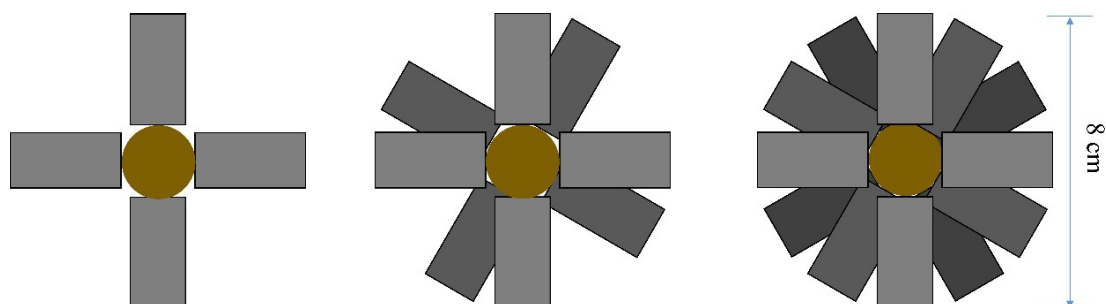


Fig S23. The three layer of "adsorbent leaves" of the "sorption tree" in configuration I.

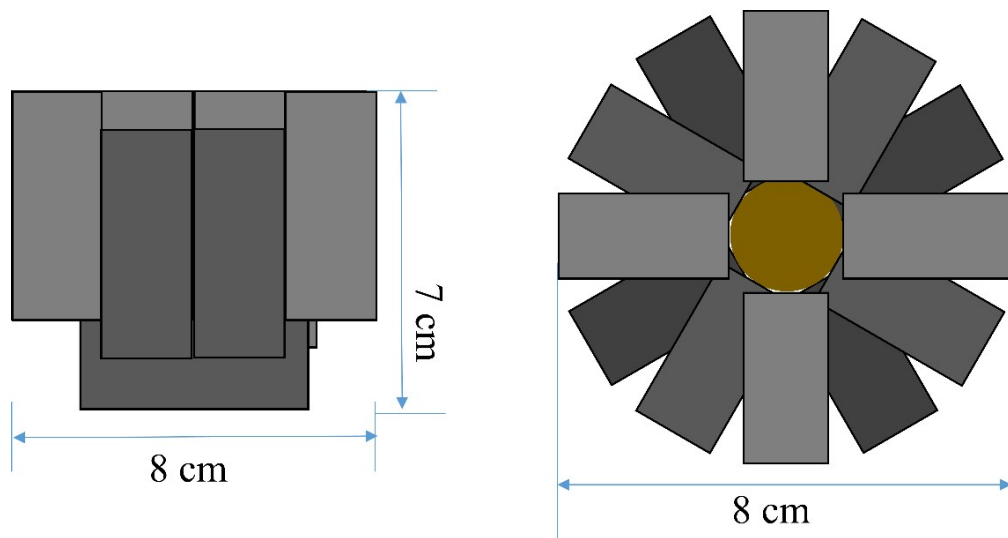


Fig S24. The projected areas of the “sorption plane” and the “sorption tree” in configuration I.

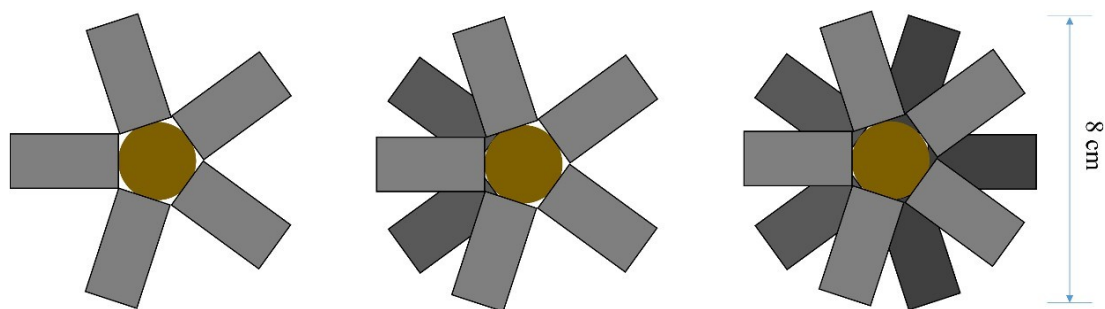


Fig S25. The three layer of “adsorbent leaves” of the “sorption tree” in configuration II.

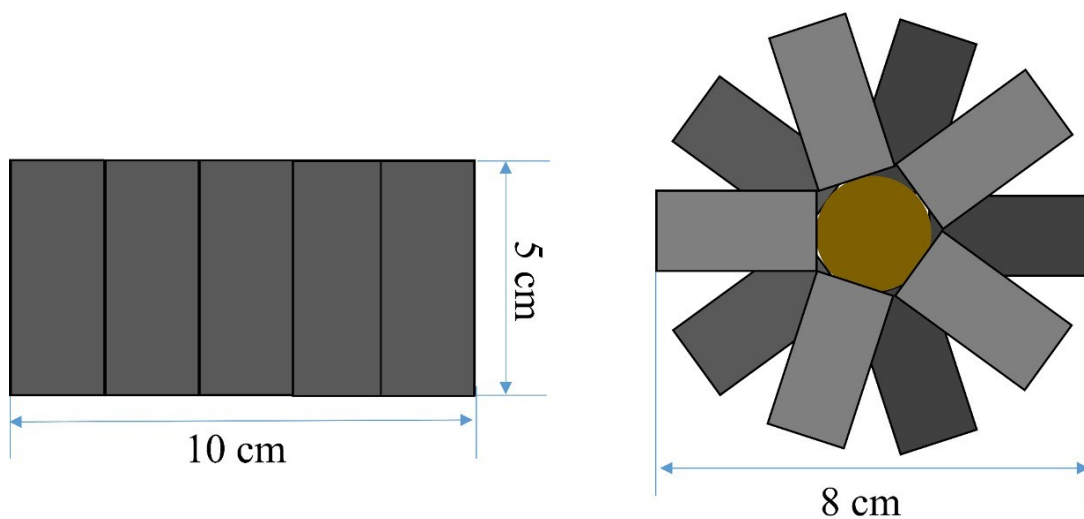


Fig S26. The projected areas of the “sorption plane” and the “sorption tree” in configuration II.

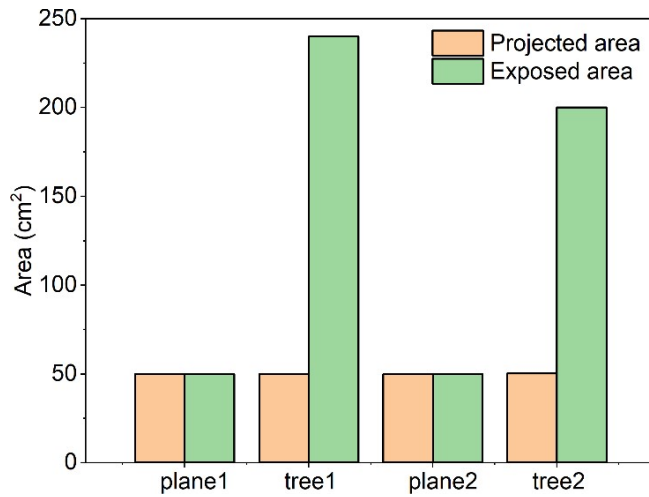


Fig S27. The comparison between projected area and exposed area for the “sorption plane” and the “sorption tree” by different configuration (I and II).

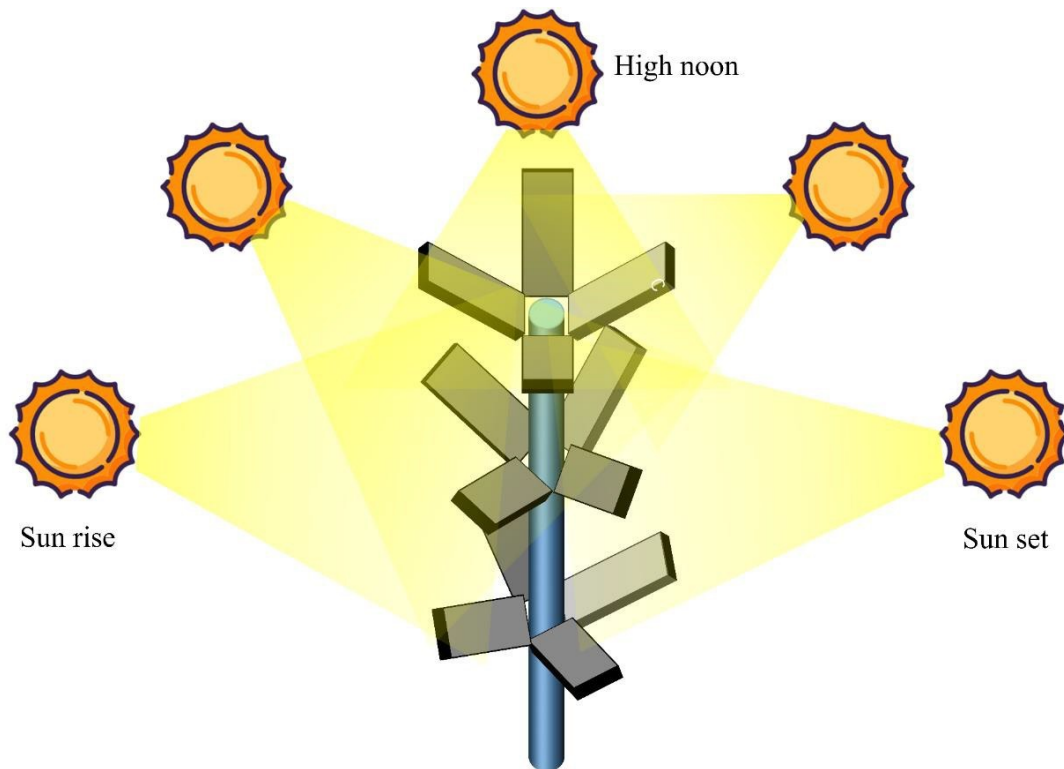


Fig S28. The illustration figure which shows the sunlight absorption process for the “sorption tree” in all direction when the sun moves to the variable attitude.

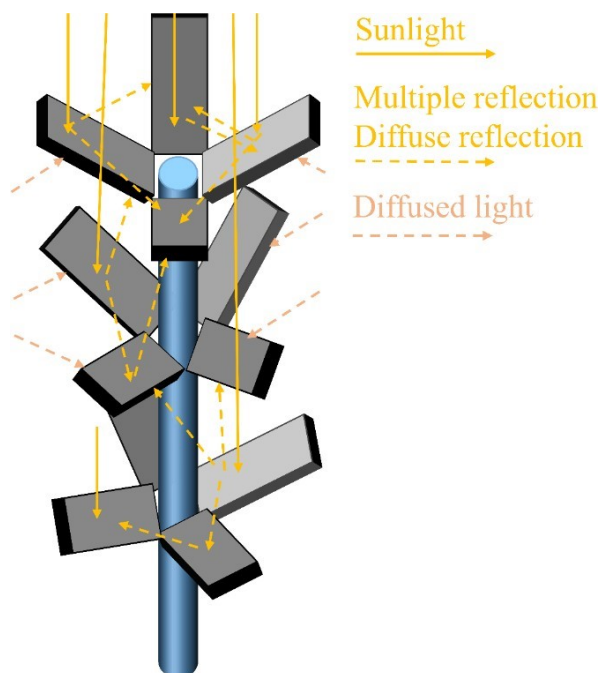


Fig S29. The illustration figure which shows the sunlight absorption process for the “sorption tree”. It can absorb sunlight and diffused light directly, and go through the multiple reflection, diffuse reflection, all of which are beneficial to the solar utilization of the “sorption tree”.

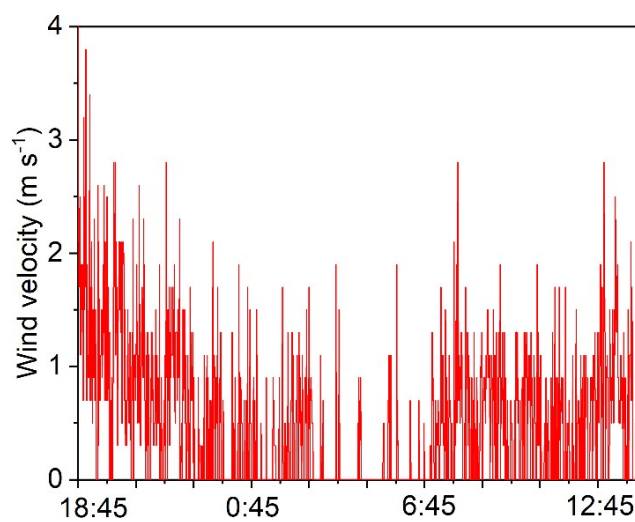


Fig S30. The wind velocity on the roof of our laboratory when the open adsorption and desorption experiment is conducted.

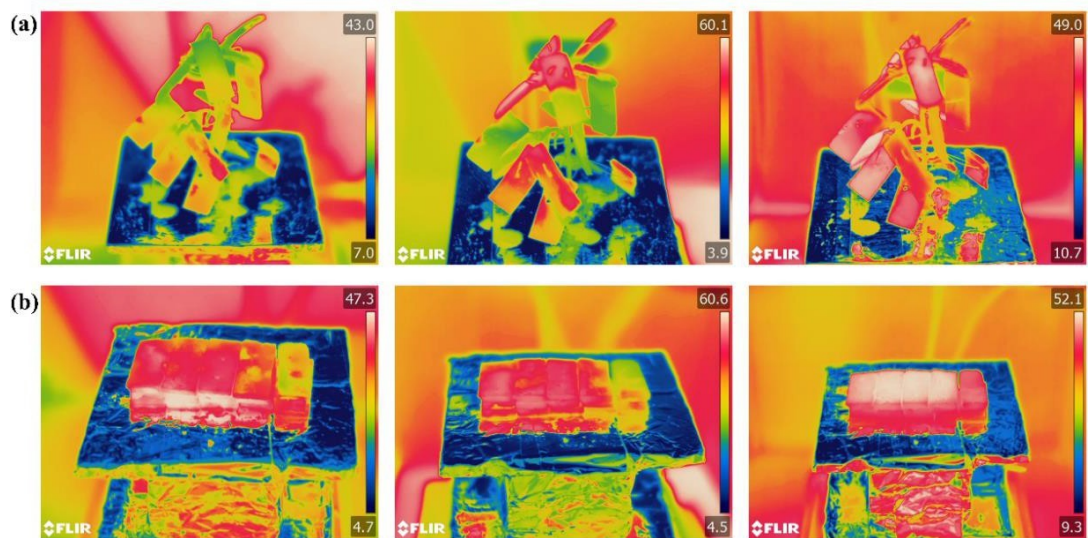


Fig S31. The IR photographs of (a) the “sorption tree” and (b) the “sorption plane” during the desorption experiment. They present the temperature distribution for the sorption beds from 8:00 am, 11:00 am, and 2:00 pm.

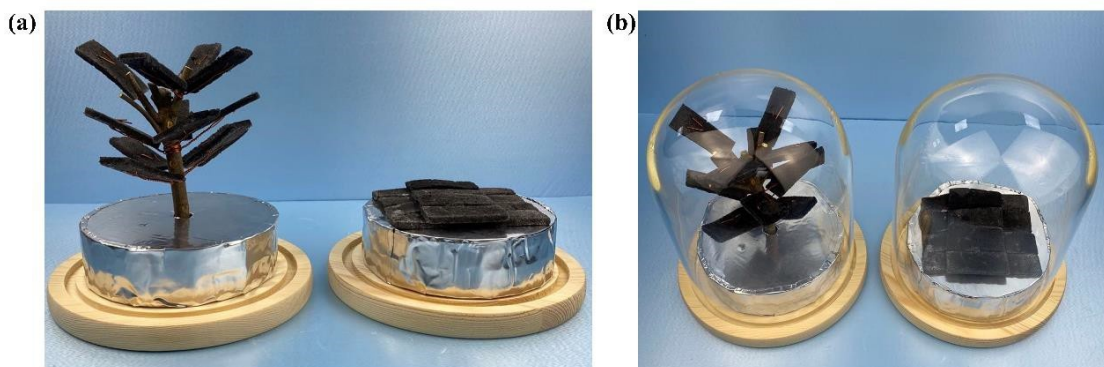


Fig S32. The photographs of device for the “sorption tree” and the “sorption plane”, both of which include the same mass of IMFCAs and the same projected area. (a) the arrangements for the two configurations during the adsorption process at night; (b) the devices for the two configurations during the desorption process in the daytime.



Fig S33. The photograph of device for the “sorption tree” and the “sorption plane” during the desorption process under the sunlight.

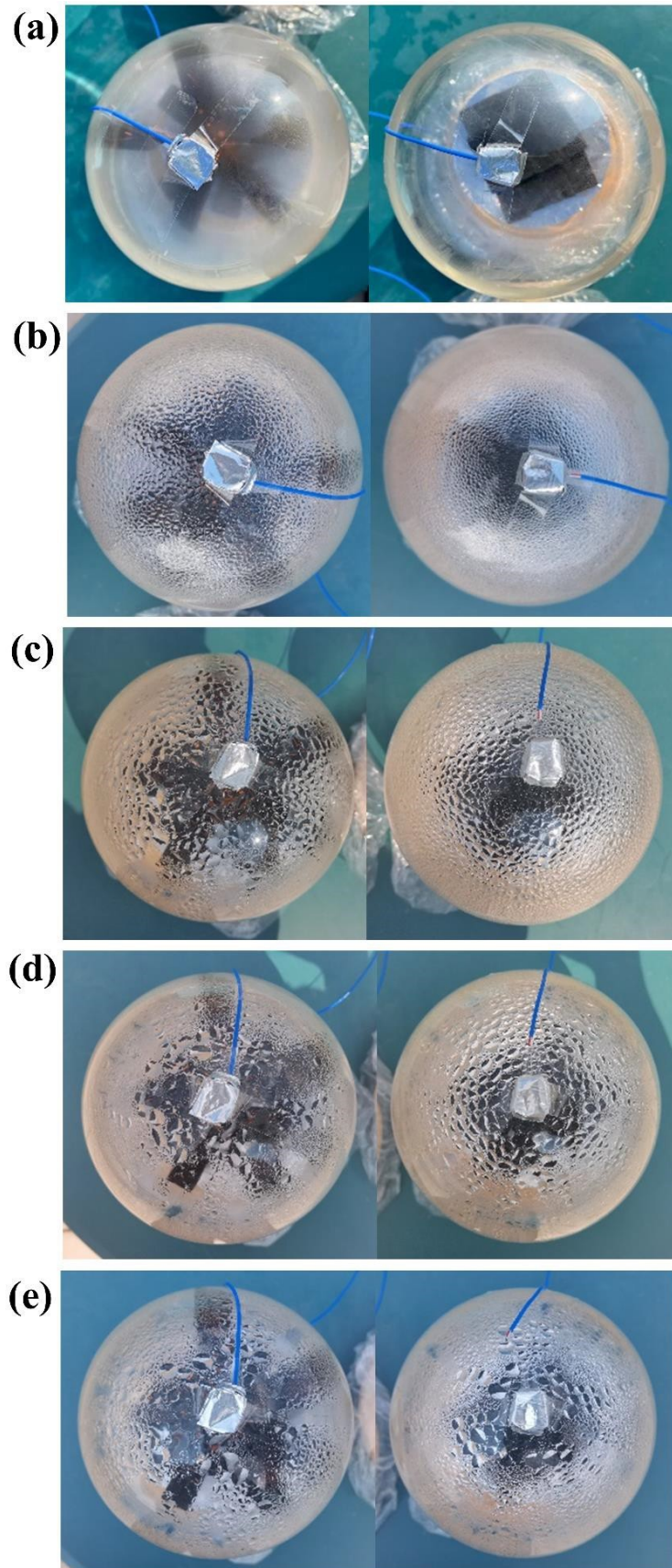


Fig S34. The photograph about the water droplets in the “sorption tree” and the “sorption plane” during the desorption process at (a)7:45 am, (b) 8:45 am, (c) 9:45 am, (d) 10:45 am, (e) 11:45 am.

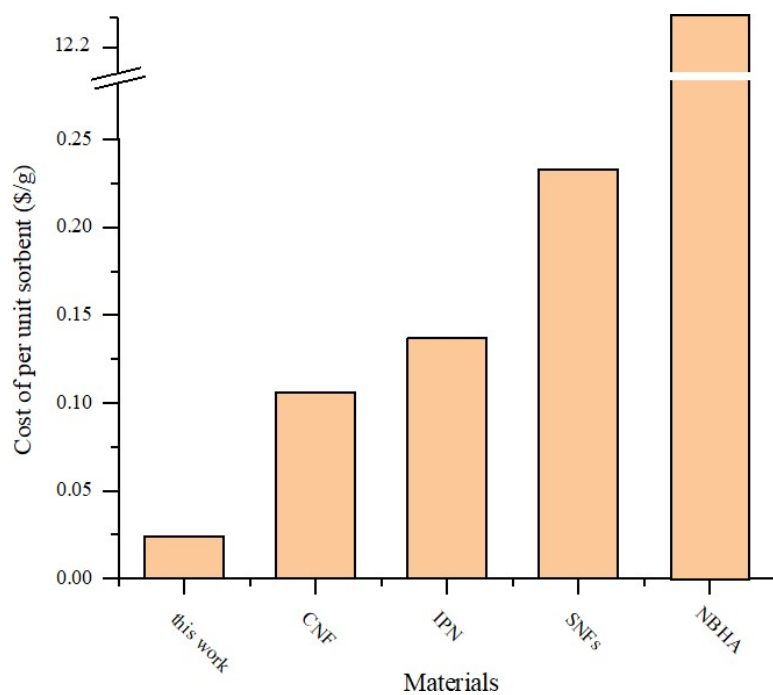


Fig S35. The comparison related to the material's costs of several excellent adsorbents in recent literature.

Table S1. The component for IMFCA with different immersed CaCl₂ concentration

| CaCl ₂ (aq) | 10 wt. % | 20 wt. % | 30 wt. % | 40 wt. % |
|------------------------------|----------|----------|----------|----------|
| MF(g) | 0.063 | 0.065 | 0.0604 | 0.612 |
| IMFSA(g) | 0.264 | 0.268 | 0.264 | 0.277 |
| IMFCA(g) | 1.076 | 1.78 | 3 | 3.698 |
| Percent of MF | 5.86% | 3.65% | 2.02% | 1.65% |
| Percent of SA-Ink | 24.54% | 15.06% | 8.8% | 7.49% |
| Percent of CaCl ₂ | 69.6% | 81.29% | 89.18% | 90.86% |

Table S2. The cost calculation for IMFCA with immersed CaCl₂ concent of 20 wt. %

| Name | MF | CaCl ₂ | SA(s) | Ink(s) |
|---------------------------------------|------------------------------------------------------------------------------------|-------------------|--------|--------|
| Percent | 3.65% | 81.29% | 10.69% | 4.37% |
| Price per mass (\$ kg ⁻¹) | 18.67 | 0.20 | 0.44 | 20 |
| Price of IMFCA (\$ kg ⁻¹) | 1.765 | | | |
| Water uptake for IMFCA | RH30%: 2.94 \$ kg ⁻¹ of water; RH60%: 1.26 \$ kg ⁻¹ of water | | | |
| “Sorpton tree” | 0.329 \$ kg ⁻¹ of water | | | |
| “sorpton plane”- | 0.66 \$ kg ⁻¹ of water | | | |

Note: The price of every raw material has been obtained from <https://www.1688.com>. In the SA solution mixed with carbon ink, the ratio of SA solution to the carbon ink is 10:1. By calculating according to the concentration of these solution, the ratio of SA to solid matter in carbon ink is about 2.448:1 for the mixed solution. The price for IMFCA to produce water is calculated by the water uptake of IMFCA in a single-day cycle in the specific condition. Similarly, the price to produce water in “sorpton tree” or “sorpton plane” is calculated according to the experimental result in Section 2.5: ~ 15 g of IMFCA in “sorpton tree” collected ~80.54 g of water, while ~15 g of IMFCA in “sorpton plane” obtained ~40.03 g of water.

Table S3. The comparison of sorption capacity for various sorbents

| Sorbent | Sorption capacity at 25 °C (g g ⁻¹) | | | Reference |
|---------------------------|-------------------------------------------------|-------------|------------|------------------|
| | RH30% | RH60% | RH80% | |
| IMFCA | 0.63 | 1.38 | 2.3 | this work |
| MnO ₂ | 0.1 | 0.13 | 0.18 | 1 |
| [EMIM][AC] | 0.23 | 0.63 | 1.18 | 2 |
| HCS-LiCl | 0.58 | 1.12 | 2.2 | 3 |
| PGF | -- | 0.64 | 2.1 | 4 |
| Cu(ii)-ethanolamine | 0.14 | 0.61 | 1.25 | 5 |
| PAM-CNT-CaCl ₂ | -- | 1.08 | 1.73 | 6 |
| IPN(Alg-Ca-PNIPAM) | 0.18 | 0.31 | 0.48 | 7 |
| G-PDDA | 0.13 | 0.37 | 0.7 | 8 |
| ZnO _x hydrogel | 0 | 0.2 | 0.6 | 9 |
| Co-SHM | 0.11 | 0.71 | 1.9 | 10 |
| MOF-801 | 0.27 | 0.34 | 0.36 | 11 |
| MOF-303 | 0.34 | 0.42 | 0.45 | 12 |
| MIP-200 | 0.4 | 0.43 | 0.45 | 13 |
| UiO-66 | 0.1 | 0.41 | 0.43 | 14 |
| MOF-841 | 0.43 | 0.48 | 0.49 | 15 |
| CAU-10 | 0.3 | 0.31 | 0.32 | 16 |
| CNF monolith | 0.4 | 0.8 | -- | 17 |
| SNFs | 0.1 | 0.58 | 0.68 | 18 |

Note: it is reported that when relative humidity (RH) is above 80%, water harvesting based on sorption has no advantage compared with fog or dew collection¹⁹. Therefore, in this table, we just choose three kinds of typical conditions below RH85%, which separately represent the low, medium, and the high humid areas. Apparently, our IMFCA is most promising to apply in wide humid range in terms of sorption capacity.

Table S4. the solar conversion efficiency in outdoor experiment

| Day | 23 th | 24 th | 25 th | 26 th | 27 th |
|-----------------------------------------------|------------------|------------------|------------------|------------------|------------------|
| Total solar irradiation (kJ) | 124.75 | 93.35 | 104.6 | 122.65 | 101.3 |
| $\eta_{\text{conv_tree}}$ | 39.3% | 58.6% | 43.5% | 37.4% | 48.6% |
| $\eta_{\text{conv_plane}}$ | 17.5% | 28.6% | 31.6% | 27.5% | 32.3% |
| Improvement (times) | 2.2 | 2.0 | 1.4 | 1.4 | 1.5 |

Note: As for the desorption process of our device, the solar conversion efficiency could be calculated by the equation:

$$\eta_{\text{conv}} = \frac{(H_v + H_s) \times m_{\text{de}}}{G} \quad (\text{a})$$

$$H_s = (c_{p,l} - c_{p,v}) \times (T_b - T_{\text{sur}}) \quad (\text{b})$$

η_{conv} is the solar conversion efficiency of the desorption experiment, H_v is the heat of vaporization, H_s is the sensible heat of water, m_{de} is the mass change during the desorption process, G is the total solar irradiation; $c_{p,l}$ and $c_{p,v}$ are the specific heat of liquid water and water vapor, respectively, T_{sur} is the temperature of samples' surface, T_b is the boiling temperature.

From the table, by the sorption-tree design the solar conversion efficiency has improved 1.4-2.2 times. Attributed to the three-dimensional tree shape, both the sorption kinetics and the sunlight absorption of SAWH device have been enhanced, which contributes to the high solar conversion efficiency.

Secondly, we can find that the solar conversion efficiency of sorption-tree is no more than 60%. It is because that in the outdoor experiment the device presents high desorption rate in the preliminary stage and completes desorption almost in the morning, which means the vast waste of solar energy in the afternoon. Therefore, the multiple cycles of adsorption-desorption process in the whole day is also pivotal to utilize solar energy more sufficiently. In the future, combining the sorption-tree and multiple cycles for SAWH technology will further promote the solar utilization efficiency.

Table S5. The indicates of SAWH performance in outdoor experiment

| | Day | 23 th | 24 th | 25 th | 26 th | 27 th |
|-------|-----------------------------------------------|------------------|------------------|------------------|------------------|------------------|
| tree | SWP (g g ⁻¹ _{adsorbent}) | 1.08 | 1.24 | 1.020 | 0.95 | 1.08 |
| | η_{de} | 63.9% | 67.3% | 68.0% | 69.2% | 70.2% |
| | R _{col} | 53.5% | 57.9% | 57.9% | 54.3% | 58.5% |
| | WPA (kg m ⁻² day) | 3.24 | 3.72 | 3.064 | 2.844 | 3.24 |
| plane | SWP (g g ⁻¹ _{adsorbent}) | 0.4 | 0.49 | 0.63 | 0.57 | 0.58 |
| | η_{de} | 60.3% | 50.0% | 61.2% | 61.9% | 58.8% |
| | R _{col} | 41.8% | 35.0% | 44.2% | 39.3% | 39.5% |
| | WPA (kg m ⁻² day) | 1.2 | 1.48 | 1.89 | 1.7 | 1.74 |

Note: The specific water productivity per cycle (SWP) could be calculated by:

$$SWP = \frac{m_{col}}{m_s} \quad (c)$$

m_{col} denotes the mass of collected water and m_s denotes the mass of adsorbent.

The desorption efficiency η_{de} could be calculated by:

$$\eta_{de} = \frac{m_{de}}{m_{ad}} \quad (d)$$

m_{ad} is the mass of water uptake during adsorption process.

The ratio of collected over adsorbed water (R_{col}) could be calculated:

$$R_{col} = \frac{m_{col}}{m_{ad}} \quad (e)$$

The water productivity per projected area (WPA) could be calculated:

$$WPA = \frac{m_{col}}{A \cdot \tau} \quad (f)$$

A is the area of the top surface of samples, τ is the time of AWH experiment.

Table S6. The comparison of cost in recent literature

| material name | IMFCA | CNF | IPN | SNFs | NBHA |
|-------------------------------------------------|-----------|--------|--------|---------|----------|
| MC(\$ g ⁻¹) | 0.024 | 0.11 | 0.14 | 0.23 | 12.26 |
| m _a -25°C, RH30%(g g ⁻¹) | 0.63 | 0.5 | 0.18 | 0.1 | 0.6 |
| m _a -25°C, RH60%(g g ⁻¹) | 1.38 | 0.8 | 0.3 | 0.58 | <4 |
| UCW-RH30%(\$ g ⁻¹) | 38.22 | 212.00 | 760.61 | 2331.40 | 20430.33 |
| UCW-RH60%(\$ g ⁻¹) | 17.45 | 132.50 | 456.37 | 401.97 | >3064.55 |
| Reference | This work | 17 | 7 | 18 | 19 |

Note: MC denotes the cost of adsorbent material (dollar per gram adsorbent), m_a denotes the water uptake (gram per gram adsorbent), and UCW denotes the cost for adsorbing 1 gram of water in single cycle (dollar per gram adsorbed water).

From table S6, the cost of adsorbent material for IMFCA is only 1%~1‰ of other adsorbents. As for the SAWH capacity, the material's unit water uptake could represent the ideal systemic performance for SAWH device. On the one hand, this table shows that the water uptake of IMFCA is 1-6 times superior to other adsorbents. On the other hand, our sorption-tree system can exert IMFCA's unit capacity almost all rather than other reported conventional devices.

Hence, in system level, compared to recent promising researches the sorption-tree with IMFCA as the adsorbent-leaf has double superiority, attributed to the excellent IMFCA and prospective three dimensional tree-like design.

Reference:

1. J. Wang, Y. Dang, A. G. Meguerdichian, S. Dissanayake, T. Kankanam-Kapuge, S. Bamonte, Z. M. Tobin, L. A. Achola and S. L. Suib, *Environmental Science & Technology Letters*, 2019, **7**, 48-53.
2. H. Qi, T. Wei, W. Zhao, B. Zhu, G. Liu, P. Wang, Z. Lin, X. Wang, X. Li, X. Zhang and J. Zhu, *Adv Mater*, 2019, **31**, e1903378.
3. R. Li, Y. Shi, M. Wu, S. Hong and P. Wang, *Nano Energy*, 2020, **67**.
4. H. Yao, P. Zhang, Y. Huang, H. Cheng, C. Li and L. Qu, *Adv Mater*, 2020, **32**, e1905875.
5. J. Yang, X. Zhang, H. Qu, Z. G. Yu, Y. Zhang, T. J. Eey, Y. W. Zhang and S. C. Tan, *Adv Mater*, 2020, DOI: 10.1002/adma.202002936, e2002936.
6. R. Li, Y. Shi, M. Alsaedi, M. Wu, L. Shi and P. Wang, *Environ Sci Technol*, 2018, **52**, 11367-11377.
7. K. Matsumoto, N. Sakikawa and T. Miyata, *Nat Commun*, 2018, **9**, 2315.
8. K. Yang, T. Pan, I. Pinnau, Z. Shi and Y. Han, *Nano Energy*, 2020, **78**.
9. D. K. Nandakumar, Y. Zhang, S. K. Ravi, N. Guo, C. Zhang and S. C. Tan, *Adv Mater*, 2019, **31**, e1806730.
10. X. Zhang, J. Yang, R. Borayek, H. Qu, D. K. Nandakumar, Q. Zhang, J. Ding and S. C. Tan, *Nano Energy*, 2020, **75**.
11. H. Kim, S. R. Rao, E. A. Kapustin, L. Zhao, S. Yang, O. M. Yaghi and E. N. Wang, *Nature Communications*, 2018, **9**, 1191.

12. N. Hanikel, M. S. Prevot, F. Fathieh, E. A. Kapustin, H. Lyu, H. Wang, N. J. Diercks, T. G. Glover and O. M. Yaghi, *ACS Cent Sci*, 2019, **5**, 1699-1706.
13. S. Wang, J. S. Lee, M. Wahiduzzaman, J. Park, M. Muschi, C. Martineau-Corcos, A. Tissot, K. H. Cho, J. Marrot, W. Shepard, G. Maurin, J. S. Chang and C. Serre, *Nature Energy*, 2018, **3**, 985-993.
14. H. Furukawa, F. Gandara, Y. B. Zhang, J. Jiang, W. L. Queen, M. R. Hudson and O. M. Yaghi, *J Am Chem Soc*, 2014, **136**, 4369-4381.
15. J. Xu, T. Li, J. Chao, S. Wu, T. Yan, W. Li, B. Cao and R. Wang, *Angew Chem Int Ed Engl*, 2020, **59**, 5202-5210.
16. X. Liu, X. Wang and F. Kapteijn, *Chem Rev*, 2020, **120**, 8303-8377.
17. Y. Chen, Z. Yu, Y. Ye, Y. Zhang, G. Li and F. Jiang, *ACS Nano*, 2021, **15**, 1869-1879.
18. S. Kim, H. Park and H. Choi, *Microporous and Mesoporous Materials*, 2019, **281**, 23-31.
19. M. Wang, T. Sun, D. Wan, M. Dai, S. Ling, J. Wang, Y. Liu, Y. Fang, S. Xu, J. Yeo, H. Yu, S. Liu, Q. Wang, J. Li, Y. Yang, Z. Fan and W. Chen, *Nano Energy*, 2021, **80**.